

Influence of multiscale surface roughness on permeability in fracturesZhongzheng Wang ^{1,2,3} Yanyao Bao,¹ Jean-Michel Pereira ²
Emilie Sauret ³ and Yixiang Gan ^{1,4,*}¹*School of Civil Engineering, The University of Sydney, New South Wales 2006, Australia*²*Navier, Ecole des Ponts, Univ. Gustave Eiffel, CNRS, Marne-la-Vallée 77420, France*³*School of Mechanical, Medical and Process Engineering, Faculty of Engineering, Queensland University of Technology, Brisbane QLD 4001, Australia*⁴*The University of Sydney Nano Institute (Sydney Nano), The University of Sydney, New South Wales 2006, Australia*

(Received 27 August 2021; accepted 21 January 2022; published 3 February 2022)

We systematically study the role of surface roughness in fluid flow through rough fractures by using direct numerical simulations. Random rough fractal surfaces are generated with different relative roughness, which are then decomposed using the wavelet analysis method. Different frequencies of surface topological information is filtered in a level-by-level procedure, while the large-scale waviness remains approximately unchanged. To explore the effects of surface roughness across a spectrum of length scales, simulations are carried out for each approximation level under different flow conditions and fracture spacing. Our results reveal the impact of relative roughness and roughness details at different length scales on the nonlinear flow behavior due to inertia associated with the formation of eddy flows. We further propose an error index to describe the relative error in permeability induced by limited resolution in surface profile description. Our analysis shows that the relative error in permeability from surfaces under different levels of approximation and relative roughness can be well described by the proposed index for a wide range of flow conditions and fracture apertures. This study provides insights into the role of multiscale roughness on the fluid flow through rough fractures.

DOI: [10.1103/PhysRevFluids.7.024101](https://doi.org/10.1103/PhysRevFluids.7.024101)**I. INTRODUCTION**

Flow through rough fracture is involved in many geological and geotechnical applications, such as petroleum reservoir exploitation and CO₂ geosequestration [1–6]. Therefore, understanding fluid flow through a rough-walled fracture is of great importance for accurate modeling and interpretation of energy- and mass-transport processes through fractured networks.

Despite that the flow through rough fracture can be fully described by the Navier-Stokes equations (NSEs), the nonlinear term due to inertia makes the equation difficult to solve. To circumvent this problem, simplification of the NSE is applied, such as ignoring the inertia term when the advective inertial forces are insignificant compared with viscous forces, i.e., Reynolds number $Re \ll 1$, which leads to the Stokes equation [7–11]. With further simplification based on the geometrical assumption according to which the variation of fracture aperture is gradual, the Stokes equation can be reduced to the Reynolds equation (or the local cubic law). Due to its simplicity, the Reynolds equation has been extensively applied in quantifying fluid flow through rough fractures in many practical situations [9,12–15]. Nevertheless, the applicability and validity of local cubic law are limited due to the presence of roughness and/or the effect caused by inertial force, which is

*yixiang.gan@sydney.edu.au

reflected by the overestimation of flow rate compared with experimental observations and numerical simulations [13,14,16–19].

With the development of numerical methods based on solving the nonlinear NSE, progress has been made to understand the impact of surface roughness on fluid flow through rough fractures [11,17,18,20–22]. At low Reynolds number, the flow is expected to obey Darcy’s law, i.e., a linear relationship between the flux and pressure gradient. At higher flow rate, due to the more dominant inertial effects, a pressure drop proportional to the velocity squared is expected [17]. In the seminal work by Brown *et al.* [23], with the fracture roughness represented by sinusoidal curves, it was shown that the overestimation of transmissivity as per the Reynolds equation increases with greater relative roughness and Reynolds number, indicating the enhanced energy dissipation due to the presence of roughness. Based on real rock samples, an earlier onset of deviation from the Darcy-type flow as the pressure gradient increases is observed for fractures with greater relative roughness [22]. For the random rough surface in rock fractures, the roughness can be characterized by the large-scale waviness and small-scale unevenness, which are also called the primary and secondary roughness [24,25]. Based on this understanding, Zou *et al.* [20] adopted the wavelet analysis technique for roughness decomposition to investigate the effects of different scales of roughness on nonlinear flow behavior in two-dimensional (2D) rough fractures. The authors revealed the significant role of secondary roughness on generating eddy flow, which consequently causes a decrease in permeability. Liu *et al.* [22] further conducted three-dimensional (3D) simulations using the lattice Boltzmann method for detailed quantification of effects of multiscale surface roughness on the flow behavior in rough fractures.

The framework of using wavelet analysis for roughness decomposition and subsequent numerical simulations offers an effective way for quantitative investigation of how different scales of roughness impact the flow in rough fractures. However, one of the key issues is the proper definition of the cutoff length separating the low-frequency waviness (general shape of fracture) and the high-frequency unevenness (white noise). The current criterion as in Refs. [20,22] is based on the variance of the surface profile, i.e., the variance of the primary roughness should be “approximately” constant as the original surface profile, whereas a rigorous mathematical definition is missing. We note that the criterion is purely a geometric consideration of the surface profile and independent of fracture aperture and flow conditions. However, by decomposing the original surface profile into two distinct surface profiles, i.e., the primary and secondary roughness [20,22], the effect of surface features associated with different length scales, i.e., different approximation levels (or, cutoff-length), remain unexplored. Another challenging aspect is the quantitative description of the error in permeability when certain high-frequency roughness is ignored, where the error is the discrepancy between the apparent permeability measured in fractures with limited resolution (e.g., resolution in 3D printing for experiments, or mesh size in numerical simulations) and the true permeability in original fractures. In this work, the wavelet analysis technique is used to decompose the computer-generated random fractal rough surface. Instead of decomposing the original rough surface into “primary” and “secondary” roughness using certain mathematical criterion, we probe individually the effects of roughness across a spectrum of length scales. To quantify the degree of effects from multiscale roughness, systematic direct numerical simulations are conducted across different (1) flow conditions, i.e., Re , (2) fracture spacings, i.e., relative roughness, and (3) surface profiles with different cutoff lengths, with a total of 234 sets of simulations. The influence of surface roughness at different scales is evaluated and discussed, and an error index is proposed to quantify the relative error induced when smaller-scale roughness is neglected for flow in rough fractures.

II. METHOD

Most natural surfaces and surfaces of engineering interest are self-affine across a wide range of length scales [26,27]. In this study, the self-affine fractal surface, characterized by the power spectral density (PSD) of the surface topography [26,28], is generated with a length of 50 mm and a root-mean-square roughness $R_q = 1.5$ mm. A fractal dimension $D_f = 2.3$, corresponding to

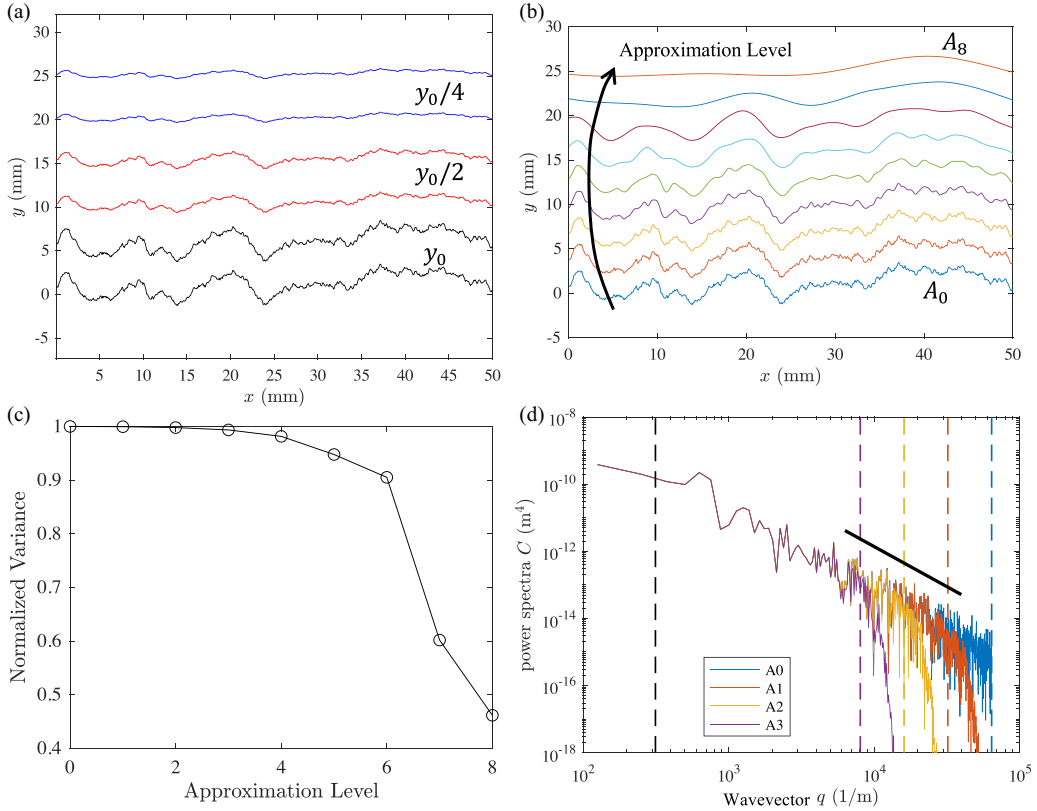


FIG. 1. Characterization of surface profile. (a) The y coordinates of the original surface y_0 is divided by two and four to generate fractures with different relative roughness. (b) From bottom to top: original (A_0) and approximated (A_1 - A_8) surface profiles using the wavelet analysis method. (c) Normalized variances of surface profiles as a function of the approximation level. (d) Power spectra of surfaces A_0 - A_3 . The black-dashed line represents the roll-off wave vector. The colored-dashed lines represent the cutoff wave vectors for each corresponding surfaces. The black-solid line corresponds to a fractal dimension $D_f = 2.30$

a Hurst exponent of 0.7, is chosen because it has been previously demonstrated that the fractal dimension of natural and artificial (polished or sandblasted) surfaces is generally less than 2.3 based on surface fragility [27]. Following the procedure in the literature [20,22], a fracture is formed by two identical rough surfaces shifted vertically by a constant distance of $H = 5$ mm, as the constant fracture aperture. To explore the effects of relative roughness defined as $r = R_q/H$, the y coordinates of the original surface profile y_0 is divided by two and four, which will be referred to as surfaces $y_0/2$ and $y_0/4$, respectively [Fig. 1(a)].

The wavelet analysis method has been widely applied in various fields of engineering and physics [29]. As mentioned by Zou *et al.* [20], different frequencies of surface topographic information from the original surface profile can be extracted by using the wavelet analysis method, which provides quantitative decomposition of the surface geometry at different frequency scales (levels) [20]. Following Wang *et al.* [21], the Db8 wavelet (Daubechies wavelet family) available in the wavelet toolbox in MATLAB is used to decompose the original surface profile in a level-by-level procedure, generating surfaces of approximation levels. In the following, the surface with approximation level M and smoothed profile by a factor of N (y coordinates divided by N) will be referred as y/N - A_M . Figure 1(b) shows the original (A_0) and decomposed (A_1 - A_8) surfaces at different approximation levels, where the surface features above a certain cutoff frequency are filtered. We refer to Ref. [20]

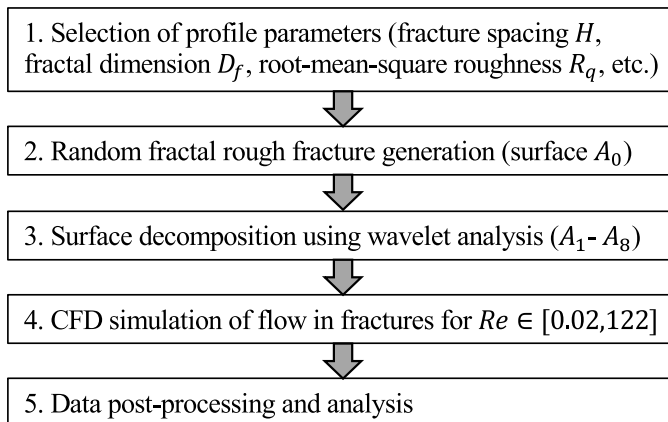


FIG. 2. A flowchart listing the key steps in this work.

for more detailed information on the wavelet analysis method. The variance of the surfaces at different decomposition levels normalized by the original surface profile is plotted in Fig. 1(c), where significant deviation of variance from the original profile ($>40\%$) is observed for A_7 and A_8 . Since the focus of the current study is to investigate the effect of surface roughness on flow in rough fractures, i.e., fine details of surface profile without changing the general shape (the dominating features of the waviness) of the surface, subsequent simulations are only conducted for surfaces A_0 - A_6 (less than 10% variation in the variance). The power spectrum of surfaces A_0 - A_3 is plotted in Fig. 1(d), with the roll-off wave vector and the cutoff wave vectors for each corresponding profiles shown as black-dashed and colored-dashed lines, respectively. The slope of the black-solid line corresponds to a Hurst exponent $H = 0.7$, or fractal dimension $D_f = 2.30$. Clearly, the power spectra generally follow the straight line in the log-log plot, indicating the fractal nature of the surface. However, beyond the cutoff wave vector, the power spectra deviate from the straight line and quickly diminishes, implying that the higher-frequency surface features are filtered in the procedure.

The numerical simulations are conducted by solving the Navier-Stokes equations using the finite-volume method (ANSYS Fluent code). No-slip boundary conditions are applied at fracture walls. Constant pressure boundary conditions are assigned at the inlet (left side) and outlet (right side), which leads to Reynolds numbers generally ranging from 0.05 to 150. The simulation is considered to reach the steady state when $|f_{i+1}/f_i - 1| < 10^{-5}$, with f the total flux at the outlet and i is the time step. For the mesh sensitivity analysis, three simulations with computation domain meshed with average grid sizes of 0.2, 0.14, and 0.1 mm are performed, where the relative differences in total flux for the former two cases based on the 0.1-mm case are 0.06% and 0.04%, respectively, implying sufficient resolution of the mesh. Finally, the average grid size of 0.14 mm was chosen for all subsequent simulations. Figure 2 shows a flowchart with the key steps in this work. Table I lists the simulation parameters.

III. RESULTS AND DISCUSSION

A. Forchheimer's law

In the regime of low flow rate with a Reynolds number typically less than 1, Darcy's law is valid for prediction of a linear relationship between the pressure gradient and flow velocity. At higher flow rates, however, the inertial forces can no longer be neglected compared with the viscous forces, and the flow will deviate from linearity due to extra energy dissipation as a result for formations of localized eddy. In this case, the flow can be described by Forchheimer's law as [30]

$$-\nabla P = aq + bq^2, \quad (1)$$

TABLE I. Simulation parameters for the current study.

Simulation parameter	Value
Fractal dimension	2.3
Relative roughness	0.075, 0.15, 0.3
Approximation levels	0, 1, 2, 3, 4, 5, 6
Liquid viscosity (kg/m s)	0.001003
Liquid density (kg/m ³)	998.2
Pressure at inlet (Pa)	1, 0.8, 0.6, 0.4, 0.2, 0.1, 0.03, 0.05,
Pressure at outlet (Pa)	0.01, 0.005, 0.001, 0.0005, 0.0001
	0

with $-\nabla P$ being the pressure gradient, q the flow rate per unit area, a and b constants, which are related to fluid property and fracture geometry [31–33], leading to the reformulated Forchheimer equation:

$$-\nabla P = \frac{\mu}{k_0}q + \beta\rho q^2, \quad (2)$$

with μ being fluid viscosity, k_0 the intrinsic permeability in Darcy regime, and β the Forchheimer coefficient. At low flow rate, the nonlinear term vanishes as β approaches zero, and Eq. (2) reduces to Darcy's law.

Figure 3(a) shows the pressure drop as a function of average velocity across different Reynolds number for the original surface y_0-A_0 . The Forchheimer equation with best fit a and b is plotted as a solid line. Note that the value of a is first fitted without consideration of the nonlinear terms using the data for $Re < 1$ (dashed line), ensuring a recovery of Darcy's law at vanishing flow rate [22]. The plot indicates that the simulation results can be well described by the Forchheimer equation, and increasing deviation from Darcy's law is observed at higher flow rate. Figures 3(c) and 3(e) plot the same relation for surfaces $y_0/2-A_0$ and $y_0/4-A_0$, respectively. It can be seen that the relative roughness in all cases impacts both the linear and nonlinear terms, with lower intrinsic permeability (represented by a) and greater nonlinear effect (represented by b) for larger relative roughness, consistent with past observations [21].

B. Transmissivity

In hydrology, transmissivity T , which is directly proportional to the hydraulic conductivity, is an important parameter for description of the liquid movement in fractures. Similar to permeability, a velocity-independent behavior of transmissivity is expected at low flow rate, i.e., the intrinsic transmissivity $T_0 = \mu/a$. With the increase of the flow rate, the apparent transmissivity T_a decreases due to the inertial effect, which can be described using the normalized transmissivity [17,21]:

$$\frac{T_a}{T_0} = \frac{1}{1 + cRe}, \quad (3)$$

where the parameter c is dimensionless. Figures 3(b), 3(d), and 3(f) plot the results of normalized transmissivity for corresponding surfaces. Curves from Eq. 3 with c chosen to optimize the fit are also plotted, which show good agreement with the values from simulations across four magnitudes of Re . The normalized transitivity remains unity, before starting to decrease at $Re = 1-10$, consistent with past experimental observations [34]. Furthermore, it can be seen that an increase in relative roughness introduces greater decrease in the apparent transmissivity as Re increases, consistent with the general trend observed in ΔP vs \bar{u}_x plots. Note that the slight deviation, especially in Fig. 3(b) in the range of $Re \in [1, 20]$, is likely due to the weak inertia regime [17,35], which predicts that

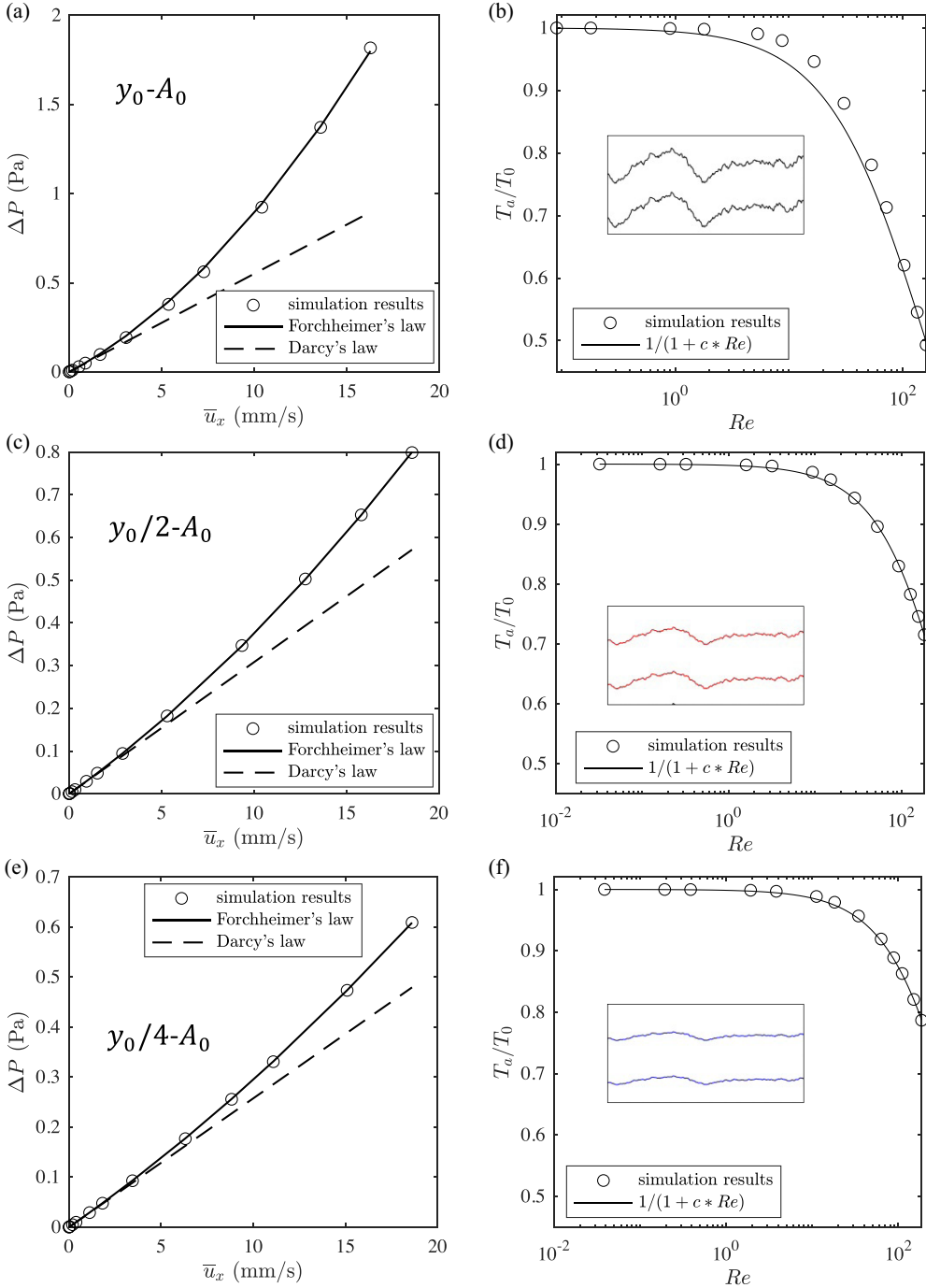


FIG. 3. Pressure drop across the fracture vs average flow velocity at steady-state for surfaces (a) y_0-A_0 , (c) $y_0/2-A_0$, and (e) $y_0/4-A_0$, with black-dashed line and black-solid lines representing Darcy's law and Forchheimer's law, respectively. Fitted values of a and b for fractures in panels (a)–(c) are $a = \{55.1, 30.8, 25.8\}$ $\text{kg/m}^3\text{s}$, and $b = \{3413, 663, 373\}$ kg/m^4 , respectively. Normalized transmissivity of flow as a function of Reynolds number for surfaces (b) y_0-A_0 , (d) $y_0/2-A_0$, and (f) $y_0/4-A_0$, with the solid curve from Eq. (3). The inset shows a subregion of the corresponding fractures.

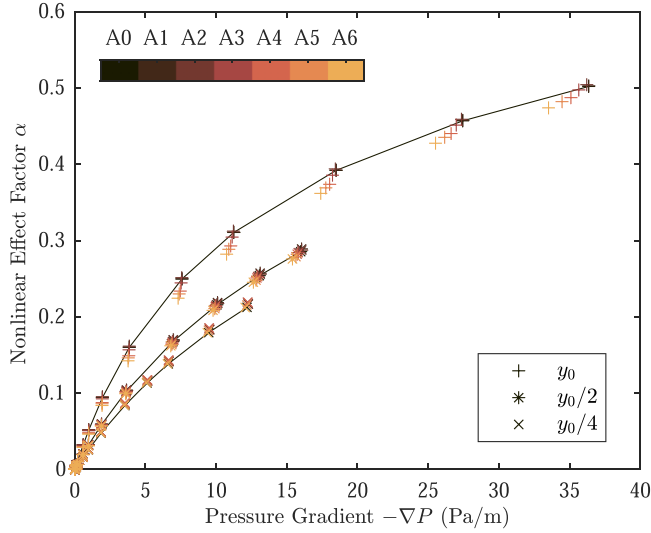


FIG. 4. Nonlinear effect factor α vs pressure gradient $-\nabla P$. Plus, star, and cross symbols are results from surfaces y_0 , $y_0/2$, and $y_0/4$, respectively, with color representing the approximation levels.

a cubic function of the flow rate is expected from the initial deviation from the linearity, instead of quadratic. To quantify the relative effect from the fluid inertia, the nonlinear effect factor α is calculated as the ratio of nonlinear pressure drop to total pressure drop [17,21,36]:

$$\alpha = \frac{bq^2}{aq + bq^2}. \quad (4)$$

Figure 4 plots the nonlinear effect factor α as a function of pressure gradient $-\nabla P$ for all surfaces of different relative roughness and approximation levels. It can be observed that α increases faster with pressure gradient for greater relative roughness. In addition, the presence of high-frequency surface features, although relatively less influential compared with relative roughness, also enhances the inertia effect.

C. Localized eddy flow

Figure 5 shows the typical velocity fields (magnitude represented by colors) and streamlines (black lines) for three representative surfaces, y_0 -A₀, y_0 -A₆, and $y_0/4$ -A₀, at low Reynolds numbers [$Re = \{0.045, 0.069, 0.019\}$], respectively, as in Fig. 5(a) and high Reynolds numbers [$Re = \{81, 122, 93\}$], respectively, as in Fig. 5(b). Note that the Reynolds number are not identical since the constant pressure boundary conditions are applied.

For the surface profile y_0 -A₀, the formation of different sizes of eddy flow can be observed at high Re , whereas the flow generally remains laminar at low Re . When the high-frequency feature of the roughness is removed, as in y_0 -A₆, in spite of observation of eddy flow at high Re , greater “smoothness” of the streamline of eddies are observed compared with a rougher surface. For the surface $y_0/4$ -A₀, however, the flow remains largely laminar at both low and high Re . Figure 5 qualitatively demonstrates that the formation of eddy flow is collectively facilitated by an increase in relative roughness, the presence of high-frequency roughness features, and increases in Reynolds number. In particular, it is important to note the formation of small eddies even at low Re for y_0 -A₀, as in Fig. 5(a). Such formation of eddies in flow regimes with $Re \ll 1$ was also observed in numerical studies using the lattice Boltzmann method [37]. We also want to emphasize that it is likely that smaller eddy flow can be resolved with a further increase in computational resolution.

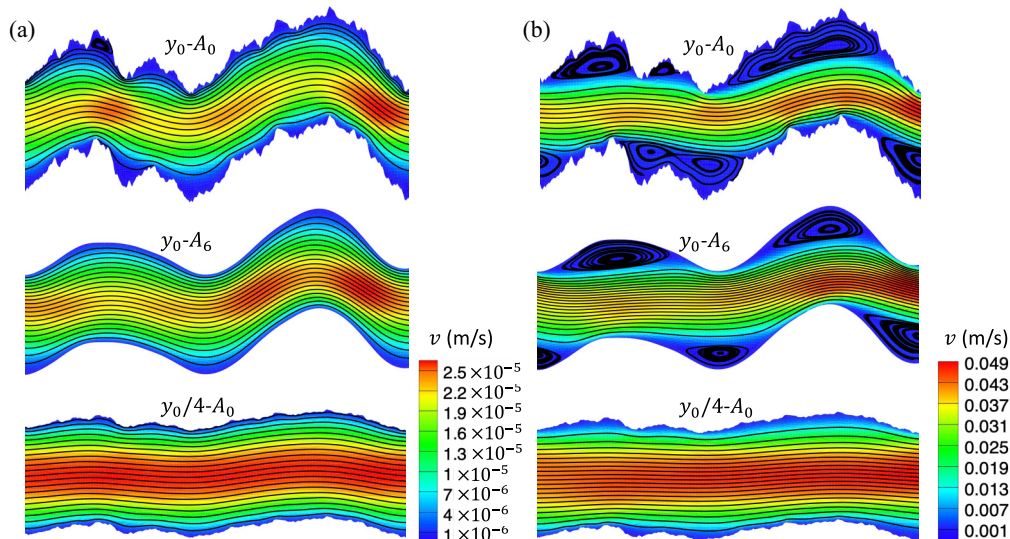


FIG. 5. Velocity fields for different surface profiles. Only a subregion of simulation domain is shown for clarity. The colorbar shows the velocity magnitude. Solid lines denote the streamlines. (a) At low Reynolds numbers. From top to bottom, $Re = \{0.045, 0.069, 0.019\}$. (b) At high Reynolds numbers. From top to bottom, $Re = \{81, 121, 93\}$.

However, the influence of these tiny eddies on the total flux in the fractures is expected to be negligible, which is similar to the argument that the impact of surface roughness on permeability below a certain cutoff length can be ignored [38,39]. These observations suggest that, although the concept of primary waviness and secondary roughness separated according to certain criterion in Refs. [20,22] is helpful for understanding the roughness effect on fluid flow in fractures, a mathematically continuous description is desired for more rigorous quantification of the roughness effect.

D. Roughness-dependent permeability

To quantitatively reveal the effects of flow condition and surface roughness on permeability, Fig. 6 shows the contour map of normalized apparent permeability k_a/k_0 , where k_a is the permeability measured at different Re and approximation levels, and k_0 is the permeability at Darcy regime without approximation [black-dashed lines in Figs. 3(a), 3(c), and 3(e)]. Two key observations

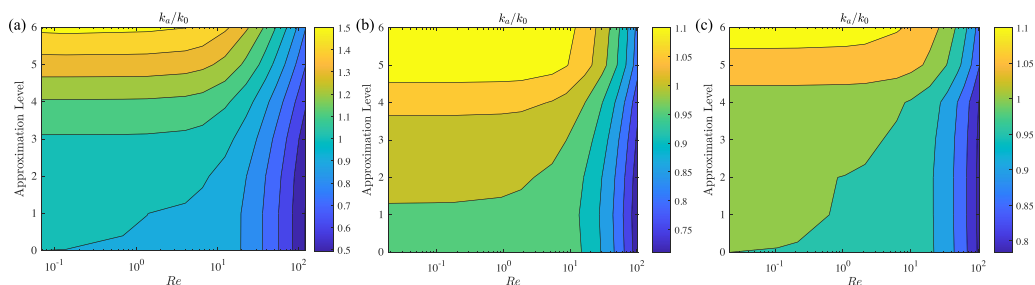


FIG. 6. Contour map of apparent permeability k_a normalized by the intrinsic permeability k_0 at different approximation levels and Reynolds numbers. (a) Surface y_0 . (b) Surface $y_0/2$. (c) Surface $y_0/4$.

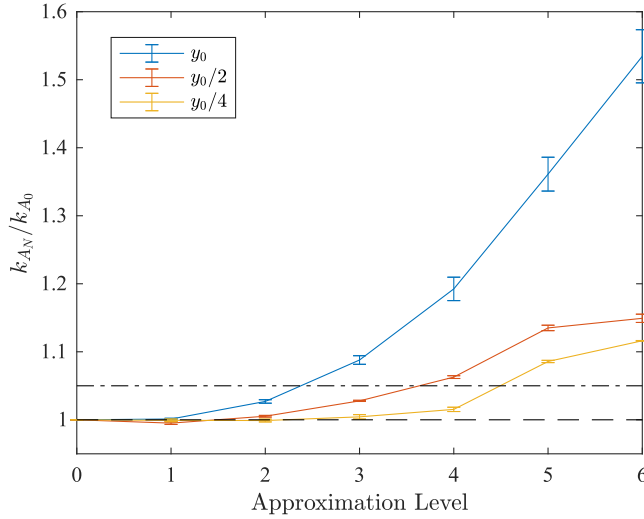


FIG. 7. Apparent permeability at different approximation levels normalized by the permeability of the corresponding surface without approximation.

from Fig. 6 include: (1) There is a competing phenomenon between the increase in approximation level, i.e., less detail on high-frequency roughness, which leads to higher apparent permeability and an increase in Re , i.e., more significant inertial effects, which leads to decrease in apparent permeability. This is reflected by the decrease in k_a from the top-left region to the bottom-right region for all three plots. (2) The influence of both roughness detail and Re on the deviation from k_0 is enhanced for greater relative roughness, according to the narrowed values of normalized apparent permeability shown in the colorbar for surfaces with decreasing relative roughness [from Figs. 6(a) to 6(c)]. As we show later, these observations also help to formulate the relation describing the deviation of permeability due to limited roughness resolution from the one for original unfiltered surface. Due to limited resolution of surface profiling equipment in experimental studies or computational resources in numerical studies, the description of the surface profile is often only down to a certain length scale. As a result, theoretical and numerical prediction of permeability for flow in rough fractures may suffer from errors due to insufficient accuracy in description of surface detail. It is thus important to quantify the error in permeability prediction under such scenarios. Here, the surface profiles without approximation, i.e., surfaces y_0-A_0 , $y_0/2-A_0$, and $y_0/4-A_0$, and the corresponding simulation results under different Re are regarded as the “ground truth.” Figure 7 plots the permeability of approximated surfaces k_{A_N} normalized by that of the original surface k_{A_0} as a function of approximation level. It is interesting to note that, for a given approximated surface, the relative deviation of permeability from the ground truth is found to remain largely unchanged at different Re , whose standard deviation is represented by the error bars in Fig. 7. Therefore, the relative errors are mainly from the description surface geometry, while being insensitive to flow conditions. For demonstration purposes, an error tolerance of 5% is chosen and shown as a black-dotted line in Fig. 7. It can be seen that the discrepancy exceeds the error tolerance at lower approximation levels for surfaces with greater relative roughness. Based on these observations, an error index can be introduced as

$$I_r = C_1 \left(\frac{y^*}{H} \right)^{C_2} e\left(-\frac{y^*}{x^*}\right), \quad (5)$$

which describes the relative error induced from the reduced resolution by ignoring the high-frequency roughness, where H is the gap between the surfaces (aperture), x^* and y^* are the

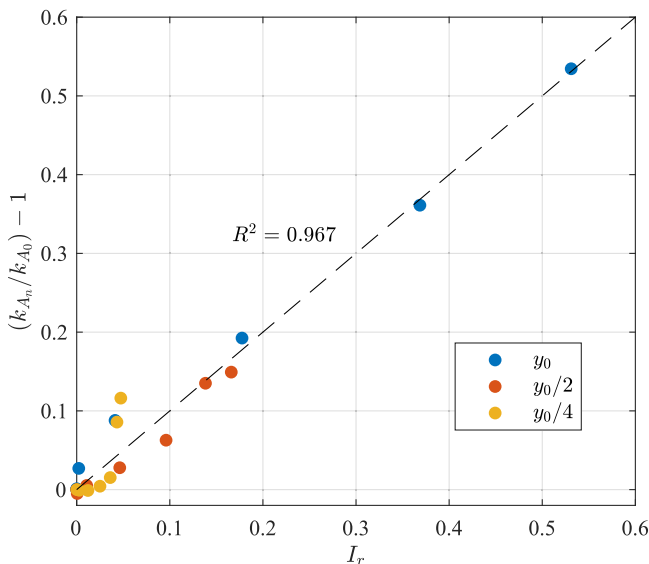


FIG. 8. Correlation between the error index I_r and calculated relative error due to limited resolution in surface profile description.

characteristic lengths of surface roughness in longitudinal and transverse direction of flow, respectively, and C_1 and C_2 are fitting parameters. The characteristic roughness in the transverse direction here is described by the root-mean-square roughness, i.e., $y^* = R_q$, which directly reflects the fluctuations of the surface perpendicular to the flow direction. The characteristic length in the longitudinal direction x^* can be directly represented by the inherent resolution of the profile along the surface. In this study, since 1024 points are used to represent the original surface with a length of 50 mm [Fig. 1(a)], x^* is therefore calculated as $50/1024 = 0.0488$ mm. In the process of roughness decomposition using the wavelet analysis technique, the high-frequency surface information is filtered out progressively by using the low-pass filter, leading to an effectively doubled wavelength of the finest surface information, which is reflected by the drastic decrease in the power spectra above corresponding wave vector, as in Fig. 1(d). This means that the longitudinal resolution can be determined by $x^* = x_0^* \times 2^n$ at approximation level n , with $x_0^* = 0.0488$ mm being the characteristic length in the longitudinal direction for the original surface. So the term y^*/H in the power-law relation in Eq. (5) is just the relative roughness, and the term y^*/x^* quantifies the relative resolution in the transverse direction with respect to the longitudinal direction. Therefore, according to Eq. (5), large error due to inadequate surface profile description is associated with (1) significant relative roughness, and (2) the actual length scale of the roughness. Particularly, I_r tends to vanish for small relative roughness y^*/H and becomes insensitive to the actual resolution of the roughness.

Using the simulation results in Fig. 7, C_1 and C_2 in Eq. (5) are fitted to be 13.5 and 1.94, respectively, with $R^2 = 0.967$. Figure 8 shows the relative error in permeability from simulation results vs I_r calculated from Eq. (5). It is found that the I_r can well describe the relative error in permeability due to limited resolution in surface profile description for all surfaces with different relative roughness and approximation levels, as indicated by collapse of points along the black-dashed line. Thus, Eq. (5) can be used to estimate the errors in numerical modeling or experiments. It can also provide guidance on the required resolution for capturing the necessary details of surface roughness, given a tolerance of relative error. For field-scale modeling, the roughness details may be ignored due to the computational constraints, while with the *a priori* knowledge of fracture morphological features, the error index in Eq. (5) can be used to estimate the upscaling deviations due to the geometric simplification for fracture networks. The insights gained in the current work

could provide the foundation for future works involving 3D numerical studies combined with experimental works.

IV. CONCLUSION

The effects of surface roughness on permeability in rough fracture are investigated by using direct numerical simulations. Random rough surfaces with controlled fractal dimension are generated with different relative roughness. The wavelet analysis technique is applied for surface decomposition, where different frequencies of surface topological information are filtered progressively in a level-by-level procedure, while the large-scale waviness (also called primary roughness profile in the literature) remain approximately constant. As opposed to past studies where the focus was placed on the primary and secondary roughness which are separated by a chosen cutoff length, here we explore the effects of surface roughness across a wide spectrum of length scales. Systematic simulations are conducted for surfaces with different relative roughness and approximation levels across a wide range of flow conditions.

The onset of nonlinear flow behavior in the pressure gradient vs flow rate curve associated with formation of eddy flow is observed as the Reynolds number increases, which can be well described by Forchheimer's law. The relative impact of inertial effect is quantified by the nonlinear effect factor. It is found that the apparent permeability becomes more sensitive to Re when roughness details of smaller scale (high-frequency roughness) are considered. Furthermore, an increase in relative roughness (smaller fracture spacing) leads to enhanced sensitivity of apparent permeability to both roughness and Re . Using the unfiltered original surface as the ground truth, the relative error on the permeability due to limited resolution in surface profile description is determined. Based on the observations of roughness effect from all simulation results, an error index is proposed to quantify the relative error in permeability prediction. It is found that the relative error in permeability from surfaces with different roughness resolutions and relative roughness can be well described by I_r .

Our study provides insights into the role of roughness of different length scales on the fluid flow through rough fractures. Given an error tolerance, the proposed error index can be a useful tool for determining the required resolution of surface profile for experimental and numerical investigations where accurate determination of permeability is needed. The improved understanding of effects of multiscale roughness on fluid flow facilitates the accurate modeling and interpretation of mass-transport processes through fractured networks.

ACKNOWLEDGMENTS

This work was financially supported by Australian Research Council (Projects DP170102886) and The University of Sydney SOAR Fellowship. Y.G. acknowledges the financial support of Labex MMCD(ANR-11-LABX-022-01) for his stay at the Laboratoire Navier at ENPC. This research was undertaken with the assistance of the HPC service at The University of Sydney.

-
- [1] R. P. Lowell, P. Van Cappellen, and L. N. Germanovich, Silica precipitation in fractures and the evolution of permeability in hydrothermal upflow zones, *Science* **260**, 192 (1993).
 - [2] A. Aydin, Fractures, faults, and hydrocarbon entrapment, migration and flow, *Mar. Pet. Geol.* **17**, 797 (2000).
 - [3] R. A. Nelson, *Geologic Analysis of Naturally Fractured Reservoirs*, 2nd ed. (Gulf Professional Publishing, Houston, Texas, 2001).
 - [4] B. Berkowitz, Characterizing flow and transport in fractured geological media: A review, *Adv. Water Resour.* **25**, 861 (2002).

- [5] S. P. Neuman, Trends, prospects and challenges in quantifying flow and transport through fractured rocks, *Hydrogeol. J.* **13**, 124 (2005).
- [6] T. Ajayi, J. S. Gomes, and A. Bera, A review of CO₂ storage in geological formations emphasizing modeling, monitoring and capacity estimation approaches, *Pet. Sci.* **16**, 1028 (2019).
- [7] P. A. Witherspoon, J. S. Y. Wang, K. Iwai, and J. E. Gale, Validity of cubic law for fluid flow in a deformable rock fracture, *Water Resour. Res.* **16**, 1016 (1980).
- [8] R. W. Zimmerman and G. S. Bodvarsson, Hydraulic conductivity of rock fractures, *Transp. Porous Media* **23**, 1 (1996).
- [9] A. P. Oron and B. Berkowitz, Flow in rock fractures: The local cubic law assumption reexamined, *Water Resour. Res.* **34**, 2811 (1998).
- [10] R. W. Zimmerman and I.-W. Yeo, *Fluid Flow in Rock Fractures: From the Navier-Stokes Equations to the Cubic Law* (American Geophysical Union, 2000), pp. 213–224.
- [11] D. J. Brush and N. R. Thomson, Fluid flow in synthetic rough-walled fractures: Navier-Stokes, Stokes, and local cubic law simulations, *Water Resour. Res.* **39**, 1085 (2003).
- [12] S. R. Brown, Fluid flow through rock joints: The effect of surface roughness, *J. Geophys. Res.* **92**, 1337 (1987).
- [13] I. W. Yeo, M. H. de Freitas, and R. W. Zimmerman, Effect of shear displacement on the aperture and permeability of a rock fracture, *Int. J. Rock Mech. Min. Sci.* **35**, 1051 (1998).
- [14] M. J. Nicholl, H. Rajaram, R. J. Glass, and R. Detwiler, Saturated flow in a single fracture: Evaluation of the Reynolds equation in measured aperture fields, *Water Resour. Res.* **35**, 3361 (1999).
- [15] A. Giacomini, O. Buzzi, A. M. Ferrero, M. Migliazza, and G. P. Giani, Numerical study of flow anisotropy within a single natural rock joint, *Int. J. Rock Mech. Min. Sci.* **45**, 47 (2008).
- [16] E. Hakami and E. Larsson, Aperture measurements and flow experiments on a single natural fracture, *Int. J. Rock Mech. Min. Sci. Geomech. Abstr.* **33**, 395 (1996).
- [17] R. W. Zimmerman, A. Al-Yaarubi, C. C. Pain, and C. A. Grattoni, Non-linear regimes of fluid flow in rock fractures, *Int. J. Rock Mech. Min. Sci.* **41**, 163 (2004).
- [18] A. H. Al-Yaarubi, C. C. Pain, C. A. Grattoni, and R. W. Zimmerman, *Navier-Stokes Simulations of Fluid Flow Through a Rock Fracture* (American Geophysical Union, 2005), pp. 55–64.
- [19] S. H. Lee, K.-K. Lee, and I. W. Yeo, Assessment of the validity of Stokes and Reynolds equations for fluid flow through a rough-walled fracture with flow imaging, *Geophys. Res. Lett.* **41**, 4578 (2014).
- [20] L. Zou, L. Jing, and V. Cvetkovic, Roughness decomposition and nonlinear fluid flow in a single rock fracture, *Int. J. Rock Mech. Min. Sci.* **75**, 102 (2015).
- [21] M. Wang, Y.-F. Chen, G.-W. Ma, J.-Q. Zhou, and C.-B. Zhou, Influence of surface roughness on nonlinear flow behaviors in 3D self-affine rough fractures: Lattice Boltzmann simulations, *Adv. Water Resour.* **96**, 373 (2016).
- [22] R. Liu, L. Yu, and Y. Jiang, Quantitative estimates of normalized transmissivity and the onset of nonlinear fluid flow through rough rock fractures, *Rock Mech. Rock Eng.* **50**, 1063 (2017).
- [23] S. R. Brown, H. W. Stockman, and S. J. Reeves, Applicability of the Reynolds equation for modeling fluid flow between rough surfaces, *Geophys. Res. Lett.* **22**, 2537 (1995).
- [24] International society for rock mechanics commission on standardization of laboratory and field tests: Suggested methods for the quantitative description of discontinuities in rock masses, *Int. J. Rock Mech. Min. Sci. Geomech. Abstr.* **15**, 319 (1978).
- [25] L. Jing, E. Nordlund, and O. Stephansson, An experimental study on the anisotropy and stress-dependency of the strength and deformability of rock joints, *Int. J. Rock Mech. Min. Sci. Geomech. Abstr.* **29**, 535 (1992).
- [26] B. N. J. Persson, O. Albohr, U. Tartaglino, A. I. Volokitin, and E. Tosatti, On the nature of surface roughness with application to contact mechanics, sealing, rubber friction and adhesion, *J. Phys.: Condens. Matter* **17**, R1 (2004).
- [27] B. N. J. Persson, On the fractal dimension of rough surfaces, *Tribol. Lett.* **54**, 99 (2014).
- [28] T. D. B. Jacobs, T. Junge, and L. Pastewka, Quantitative characterization of surface topography using spectral analysis, *Surf. Topogr.: Metrol. Prop.* **5**, 013001 (2017).
- [29] I. Daubechies, *Ten Lectures on Wavelets* (Society for Industrial and Applied Mathematics, 1992).

- [30] J. Bear, *Dynamics of Fluids in Porous Media* (American Elsevier, 1972).
- [31] M. Muskat, *Dynamics of Fluids in Porous Media* (International Human Resources Development Corporation, 1937).
- [32] L. Green, Jr., and P. Duwez, Fluid flow through porous metals, *J. Appl. Mech.* **18**, 39 (1951).
- [33] D. Cornell and D. L. Katz, Flow of gases through consolidated porous media, *Ind. Eng. Chem.* **45**, 2145 (1953).
- [34] A. H. Al-Yaarubi, C. C. Pain, C. A. Grattoni, and R. W. Zimmerman, *Navier-Stokes Simulations of Fluid Flow Through a Rock Fracture* (American Geophysical Union, 2005), pp. 55–64.
- [35] C. C. Mei and J.-L. Auriault, The effect of weak inertia on flow through a porous medium, *J. Fluid Mech.* **222**, 647 (1991).
- [36] Z. Zeng and R. Grigg, A criterion for non-Darcy flow in porous media, *Transp. Porous Media* **63**, 57 (2006).
- [37] S. Briggs, B. W. Karney, and B. E. Sleep, Numerical modeling of the effects of roughness on flow and eddy formation in fractures, *J. Rock Mech. Geotech. Eng.* **9**, 105 (2017).
- [38] S. I. R. Castillo, D. M. E. Thies-Weesie, and A. P. Philipse, Formation and liquid permeability of dense colloidal cube packings, *Phys. Rev. E* **91**, 022311 (2015).
- [39] D. Wei, Z. Wang, J.-M. Pereira, and Y. Gan, Permeability of uniformly graded 3D printed granular media, *Geophys. Res. Lett.* **48**, e2020GL090728 (2021).